*J. Fluid Mech.* (1996), *vol.* 318, *pp.* 31–47



# Hydrodynamic diffusion near solid boundaries with applications to heat and mass transport into sheared suspensions and fixed-fibre beds

By DONALD L. KOCH

School of Chemical Engineering, Cornell University, Ithaca, NY 14853, USA

(Received 29 June 1995 and in revised form 25 January 1996

Heat and mass transport in the bulk of a suspension or fixed bed in the limit of high Péclet number is controlled by hydrodynamic diffusion. This hydrodynamic diffusion is caused by the stochastic velocity field induced by the randomly distributed particles. However, the no-slip boundary conditions require that the hydrodynamic diffusivity vanish at boundaries of the medium. Thus, molecular diffusion must aid the transport in a thin boundary layer near the solid boundary. Quantitative results are derived for the hydrodynamic diffusivity, boundary layer thickness, and net resistance to transport across a dilute fixed fibrous bed in the direction transverse to the mean flow. A scaling analysis is presented for transport in the direction of the gradient of the mean velocity in a sheared suspension of neutrally buoyant spheres. This scaling analysis is able to explain the qualitative variations of the transport resistance with the Péclet number and the ratio of the suspension thickness to the particle radius.

## 1. Introduction

The rate of heat and mass transfer across a fixed bed can be enhanced greatly by fluid flow. A tracer particle passing through the medium will experience a stochastic flow resulting from the disturbances produced by the randomly positioned fixed bed particles. Thus, when the Péclet number, $Pe = U\xi/D$, is asymptotically large, one might expect that the molecular diffusivity of mass or heat, $D$, will play no role in transport. Here, $U$ is the mean velocity through the bed and $\xi$ is a length scale characteristic of the microstructure, i.e. the particle radius in a concentrated packed bed or the Brinkman screening length in a dilute fixed bed. If the effective diffusivity $D^*$ that relates the mean flux of mass across the bed to the gradient of the mean concentration is assumed to be independent of $D$ and inertial effects are negligible, then dimensional analysis implies that $D^* = d(\phi)\, U\xi$, where $d$ is a dimensionless function of the volume fraction $\phi$ and microstructure of the bed. (In this paper we will use $D^*$ to refer to the hydrodynamic diffusivity transverse to the flow and will restrict our attention to the transverse component of the effective diffusivity tensor.) This scaling analysis has been confirmed by theoretical calculations for dilute fixed beds of spheres (Koch & Brady 1985) and fibres (Koch & Brady 1986) and is in accord with experimental studies of transverse diffusion *within* a packed bed (Fried & Combarnous 1971).

However, it has been found that the heat transfer from a solid boundary *into* a packed bed is modelled more accurately if the hydrodynamic diffusivity of heat is not treated as a constant but is allowed to vary with separation from the wall (Cheng &

Zhu 1987). This variation may be expected to occur since the hydrodynamic diffusion arises from fluid velocity disturbances that must vanish at the solid boundary.

An analysis based on the method of averaged equations will be presented in §2 to elucidate the dependence of the hydrodynamic diffusivity on the distance from the wall in a fixed bed. Quantitative results will be obtained for transport across a dilute isotropic fixed fibrous bed in §2.2. However, the scaling analysis in §2.1 is also applicable to packed beds.

Hydrodynamic diffusion of heat and mass also occurs in free suspensions. A conceptually simple example is the simple shear flow of a suspension of neutrally buoyant spherical particles. If the Péclet number, $Pe_\gamma = \gamma a^2/D$, based on the shear rate $\gamma$, the sphere radius $a$ and the molecular diffusivity $D$, is asymptotically large, we may expect that the dispersion will be controlled by the stochastic hydrodynamic flow and will be independent of the molecular diffusivity. If the effective diffusivity in the bulk of the suspension is independent of the molecular diffusivity and inertial effects are negligible, then $D^* = a^2\gamma d_2(\phi)$, where $d_2$ is a dimensionless function of the particle volume fraction. The same scaling may be expected to apply to dispersion of the solid spheres themselves as to a fluid-phase tracer, albeit with a different function $d_s(\phi)$. While experimental studies (Leighton & Acrivos 1987) of the self-diffusion of a marked tracer sphere in the midst of a suspension show clear evidence for the purely hydrodynamic scaling, the results for fluid-phase tracers obtained by Wang & Keller (1985) and Sohn & Chen (1981) are more complex. The latter studies measure the rate of mass or heat transfer from one cylinder of a Couette device to the other, yielding a heat or mass transfer coefficient $h$. It is found that the Nusselt number $Nu = hH/D$ grows slightly slower than linearly with $Pe_\gamma$ and that the results depend on the ratio of the gap thickness between the two cylinders of the Couette device, $H$, to the particle radius, $a$. In §3, we will present a scaling analysis for hydrodynamic diffusion in the vicinity of a solid boundary to a sheared suspension. It will be seen that the qualitative dependence of $Nu$ on $Pe_\gamma$ and $H/a$ can be explained in terms of the resistance to transport through a boundary layer in which molecular diffusion is important.

The problems of transport across a fixed bed or particulate suspension are similar to heat and mass transport across a turbulent flow in the sense that the stochastic fluid flow enhances the transport in the bulk of the medium. This enhancement decays with proximity to a solid boundary in all three cases as a result of the no-slip boundary condition at the surface. Thus, molecular diffusion must aid the transport across a boundary layer near the surface. This phenomenon has long been appreciated for applications to heat transfer in turbulent flow (Eckert & Drake 1972), but has not been studied extensively for fixed bed and suspension flows. Of course, the nature of the stochastic flow arising in suspensions and fixed beds is quite different from a turbulent flow and we must analyse this flow and its influence on heat and mass transfer to predict the overall transport rate.

## 2. Dispersion in a dilute isotropic fibrous bed

### 2.1. *Scaling analysis*

Koch & Brady (1986) showed that the transverse hydrodynamic diffusion coefficient in the bulk of a dilute isotropic fibre bed in the limit of high Péclet number is given by

$$D^*(y \gg \xi) = D^*_\infty = \frac{9\pi^2 U a^2}{3200\xi\phi}. \tag{1}$$

Here, $y$ is the distance from the wall, $a$ is the radius of the fibre and $\xi$ is the Brinkman screening distance, which may be obtained from the following implicit relationship (Koch & Brady 1986; Spielman & Goren 1968; Howells 1974):

$$\frac{a^2}{\xi^2} = \frac{10\phi}{3[\ln(\xi/a)+\ln(2)-C]} + O\left(\frac{\phi}{\ln^3(1/\phi)}\right), \tag{2}$$

where $C = 0.577216$ is Euler's constant. Equation (1) applies at separations $y$ from the boundary of the bed that are large compared with the screening distance $\xi$, so that the wall has a negligible effect on the fluid velocity field. (Equation (1) differs from the result in Koch & Brady (1986) by a factor of $2/\pi$, owing to an algebraic error in the previous analysis.)

The order of magnitude of the bulk hydrodynamic diffusivity given by (1) may be rationalized through the following scaling analysis. $D^*$ may be estimated as the product of the rate $R$ at which a tracer molecule undergoes interactions with fibres and the square of the displacement, $\Delta y$, experienced by the tracer as a result of each interaction:

$$D^* = O(R(\Delta y)^2). \tag{3}$$

The fluid velocity disturbance, $\langle u_y' \rangle_1$, caused by a fibre begins to decay only at large distances from the fibre and is $O(f/\mu) = O(U/\ln(1/\phi))$ at separations from the fibre comparable with the screening length $\xi$. Here, $f$ is the force per unit length that the fibre exerts on the fluid, $\mu$ the fluid viscosity, $\boldsymbol{u}$ the fluid velocity, $\boldsymbol{u}' = \boldsymbol{u} - \boldsymbol{U}$ the deviation from the mean velocity, and $\langle\ \rangle_1$ indicates an ensemble average with the position and orientation of one fibre held fixed. We will use a Cartesian coordinate system with the $x$-axis parallel to the direction of the mean velocity and the $y$-axis perpendicular to both the wall and the mean flow. A tracer experiences the velocity disturbance produced by a fibre during the time $\tau = \xi/U$ required for it to be convected by the mean flow through the interaction volume surrounding the fibre. Thus, $\Delta y = f\xi/(\mu U)$. The number of fibres within an $O(\xi)$ distance of the tracer at any given time is $n\xi^2 = O(\ln(1/\phi))$, where $n = \phi/(\pi a^2)$ is the number of fibres whose axes cut a unit cross-sectional area. Since the tracer interacts with each fibre for a time $\tau$, the rate of interaction is $R = O(\phi\xi U/a^2)$. Substituting these scalings into (3) gives

$$D^*_\infty = O\left(\frac{\phi\xi^3 f^2}{Ua^2\mu^2}\right). \tag{4}$$

The Brinkman screening distance is defined in terms of the body force exerted by the fibres on the fluid, i.e. $nf = \mu U/\xi^2$. Using this relationship to eliminate $f$ from (4) gives

$$D^*_\infty = O\left(\frac{Ua^2}{\xi\phi}\right), \tag{5}$$

in agreement with (1).

Now let us consider the scaling of $D^*$ at positions close to the wall $y \ll \xi$. The unconditional ensemble-average fluid velocity, $\langle u_x \rangle$, is equal to $U$ far from the wall, i.e. for $y \gg \xi$, and goes to zero at the no-slip solid boundary to the bed. Thus, the average shear rate at the wall is $\langle\gamma\rangle = \partial\langle u_x\rangle/\partial y = O(U/\xi)$ and the average velocity near the wall is $\langle u_x\rangle = \langle\gamma\rangle y = O(Uy/\xi)$. The correlation time, defined as the time for which a tracer particle is within an $O(\xi)$ distance of a fibre, is $\tau = O(\xi/\langle u_x\rangle) = O(\xi^2/(Uy))$.

The velocity of the tracer at a position $y \ll \xi$ is influenced by all of the fibres within an $O(\xi)$ distance from the wall. Such fibres have the same $f = O(\mu U/\ln(1/\phi))$ force per unit length as fibres in the bulk of the bed to leading order, with an $O(\mu U/\ln^2(1/\phi))$

correction to this force caused by wall reflections. The velocity disturbance caused by the fibres extends over an $O(\xi)$ distance. The rate of interactions of the tracer with the fibres is $R = O(n\xi^2/\tau) = O(\phi Uy/a^2)$. The no-slip boundary condition together with the continuity equation for an incompressible fluid implies that the normal component of the fluid velocity disturbance caused by a fibre approaches zero quadratically as $y \to 0$, i.e. $\langle u_y' \rangle_1 = O(fy^2/(\mu\xi^2))$. The change in the tracer's position due to each interaction is $\Delta y = O(\langle u_y' \rangle_1 \tau) = O(fy/(\mu U)) = O(ya^2/(\xi^2\phi))$. From equation (2) it may be seen that $\Delta y/y = O(1/\ln(1/\phi)) \ll 1$ in a very dilute fibrous bed. This small displacement is a requirement for treating the transport in terms of a local relationship between the mean flux and concentration gradient occurring at $y$.

Substituting the scalings derived above into (3), the hydrodynamic diffusivity near the wall is found to be

$$D^* = \frac{d_1 Uy^3 a^2}{\phi \xi^4} = \frac{d_1' D_\infty^* y^3}{\xi^3}, \quad y \ll \xi, \tag{6}$$

where $d_1 = d_1'(9\pi^2/3200)$ is a dimensionless $O(1)$ constant. Since the hydrodynamic diffusivity approaches zero as $y \to 0$, there is a boundary layer of thickness $\delta = \xi(D/D_\infty^*)^{1/3}$ in which molecular diffusion is important even at high Péclet numbers.

In deriving (6), we have assumed that the largest contribution to the hydrodynamic diffusivity of a tracer located at $y$ comes from fibres that are an $O(\xi)$ distance from the wall. It may be shown from a similar scaling argument that the contribution to the diffusivity coming from fibres an $O(y)$ distance from the wall is asymptotically small. The velocity disturbance produced by these fibres is screened at an $O(y)$ radial separation from the fibre due to the fibre-wall interaction. As a result, the force per unit length on the fibre is $O(\mu\langle u_x \rangle/\ln(y/a)) = O(\mu Uy/[\xi \ln(y/a)])$. The velocity disturbance produced by the fibre is $\langle u_y' \rangle_1 = O(Uy/[\xi \ln(y/a)])$. The tracer interacts with a fibre for a time $y/\langle u_x \rangle = \xi/U$ and, at any given time, it is interacting with $ny^2$ near-wall fibres. Thus, the rate of interaction is $R = ny^2/\tau = \phi y^2 U/(\xi a^2)$ and the displacement per interaction is $\Delta y = \langle u_y' \rangle_1 \tau = O(y/\ln(y/a))$. The diffusivity due to near-wall fibres is found, using (3), to be $O(Uy^4\phi/(\xi a^2[\ln(y/a)]^2))$, which is smaller than the contribution of the more distant fibres accounted for in our scaling result (6) by a factor of $y/(\xi[\ln(\xi/a)/\ln(y/a)]^2)$.

We have found that the hydrodynamic diffusivity decreases in proportion to $y^3$ as the distance of the tracer from the wall decreases. The higher resistance to mass transport across the boundary layer leads to a concentration slip near the surface. For example, let us consider a situation in which the mean concentration field $\langle c \rangle$ is steady and is a function of $y$ only. In this case, the flux $Q$ is independent of $y$ and superimposing the fluxes caused by the hydrodynamic diffusivity (6) and the molecular diffusivity $D$, we have

$$Q = -D\left(d_1' \frac{y^3}{\delta^3} + 1\right)\frac{\mathrm{d}\langle c \rangle}{\mathrm{d}y}, \quad y \ll \xi. \tag{7}$$

Integrating (7), one obtains the concentration slip:

$$\Delta c \equiv \langle c \rangle (y \gg \delta) - \langle c \rangle (y = 0) = \frac{2\pi Q\delta}{3^{3/2} d_2'^{1/3} D} = \frac{2\pi Q\xi}{3^{3/2}(d_1' D_\infty^* D^2)^{1/3}}. \tag{8}$$

We can define the mass transfer coefficient as

$$h = \frac{Q}{\langle c \rangle (y = H) - \langle c \rangle (y = 0)}. \tag{9}$$

Assuming that the primary resistances to mass transfer come from the boundary layers ($y \ll \xi$ or $H-y \ll \xi$) and the bulk of the bed ($y \gg \xi$ and $H-y \gg \xi$):

$$\langle c\rangle(y=H)-\langle c\rangle(y=0)=2\Delta c+HQ/D^*_\infty, \tag{10}$$

where $Q/D^*_\infty$ is the concentration gradient in the bulk of the bed. Using (8), (9) and (10), the Nusselt number, $Nu = hH/D$, is determined to be

$$\frac{1}{Nu}=\frac{D}{D^*_\infty}+\frac{4\pi\xi D^{1/3}}{3^{3/2}H(d_1^* D^*_\infty)^{1/3}}. \tag{11}$$

The concentration slip can only be neglected compared with the $O(Q\phi\xi H/(Ua^2))$ concentration variation associated with the transport resistance, (1), across the bulk of the fibre bed when the thickness $H$ of the bed is very large, i.e. $H/a \gg (Pe_a/\phi)^{2/3}$. Here $Pe_a = Ua/D$ is the Péclet number based on the fibre radius $a$. It is interesting to note that the criterion for neglecting the concentration slip associated with the molecular-diffusion boundary layer becomes increasingly stringent as the Péclet number grows. Thus, a diffusion process that occurs purely in the bulk of the bed becomes increasingly dominated by hydrodynamic diffusion with growing Péclet number, but the transport from one boundary of the bed to the other shows the weakest dependence on molecular diffusion at an intermediate Péclet number.

The scaling analysis performed here may be applied to a concentrated packed bed of spheres of volume fraction $\phi$, provided that the screening length $\xi$ is replaced by the particle radius $a$ to reflect the fact that $a$ is the length scale over which the fluid velocity field varies in a concentrated bed. It should be noted, however, that the characteristic displacement, $\Delta y$, experienced by a tracer as a result of its interaction with each fixed sphere is $O(y)$ for $y \ll a$. Thus, one would need to adopt a spatially non-local description of the hydrodynamic diffusion process to obtain quantitative results for a packed bed. Spatially non-local transport has been discussed in other contexts by Koch & Brady (1987) and Shaqfeh (1988).

### 2.2. *Derivation of the hydrodynamic diffusivity*

Now, we turn to a quantitative determination of the hydrodynamic diffusivity near the boundary to an isotropic fixed fibre bed in the dilute limit, $\phi \ll 1$. The concentration field $c$ of a chemical tracer in the fluid phase is governed by the equation

$$\frac{\partial c}{\partial t}+\nabla\cdot(\boldsymbol{u}c-D\nabla c)=0. \tag{12}$$

We will neglect the effects of the boundary conditions on the surface of the fibres on the concentration field and simply represent the velocity disturbance of each fibre in terms of a line of point forces. It was shown by Koch & Brady (1986) that these approximations give the correct leading behaviour of the transverse effective diffusivity in the limit of high Péclet number. The ensemble average of (12) is

$$\frac{\partial\langle c\rangle}{\partial t}+\nabla\cdot[\langle\boldsymbol{u}\rangle\langle c\rangle-\langle\boldsymbol{u}'c'\rangle-D\nabla\langle c\rangle]=0, \tag{13}$$

where $\boldsymbol{u}' = \boldsymbol{u}-\langle\boldsymbol{u}\rangle$ and $c' = c-\langle c\rangle$. The ensemble average $\langle\ \rangle$ is an average over the positions and orientations of all of the fibres. We will consider an average concentration field that is independent of time and varies only in the $y$-direction. The mean velocity $\langle\boldsymbol{u}\rangle$ is a unidirectional flow in the $x$-direction. Therefore, (13) reduces to

$$\frac{\mathrm{d}}{\mathrm{d}y}\left(\langle u_y' c'\rangle-D\frac{\mathrm{d}\langle c\rangle}{\mathrm{d}y}\right)=0. \tag{14}$$

It will be seen that the average convective flux can be written as

$$\langle u'_y c' \rangle = -D^* \frac{\mathrm{d}\langle c \rangle}{\mathrm{d}y}. \tag{15}$$

Integrating (14) once using (15) gives

$$-(D+D^*)\frac{\mathrm{d}\langle c \rangle}{\mathrm{d}y} = Q, \tag{16}$$

where $Q$ is the constant flux across the bed. $D^*$ varies on an $O(y)$ length scale, cf. (6), and therefore the gradient of the average concentration, $\mathrm{d}\langle c \rangle/\mathrm{d}y$, also varies on the length scale $y$.

The mean convective flux in (15) can be obtained by averaging the conditionally averaged flux over the fibre orientation and position:

$$\langle u'_y c' \rangle = -D^* \frac{\mathrm{d}\langle c \rangle}{\mathrm{d}y} = \int \mathrm{d}\boldsymbol{e} \frac{\phi e_y}{\pi^2 a_2} \int \mathrm{d}\boldsymbol{r}_w \langle u'_y c' \rangle_1 (\boldsymbol{r} | \boldsymbol{r}_w, \boldsymbol{e}). \tag{17}$$

Here, the factor $\phi e_y/(\pi^2 a^2)$ is the number of fibres per unit area with orientation $\boldsymbol{e}$ intersecting the wall at $\boldsymbol{r}_w$. The conditional average $\langle\ \rangle_1$ is an average over the positions and orientations of all fibres except the one at $\boldsymbol{r}_w$ with orientation $\boldsymbol{e}$. By neglecting the effects of two-fibre correlations, we can approximate $\langle u'_y c' \rangle_1 \approx \langle u'_y \rangle_1 \langle c' \rangle_1$. The error incurred in making this approximation can be determined through a scaling argument analogous to that presented in §2.1. The two-fibre correlations result from fibre–fibre hydrodynamic reflections that lead to tracer displacements $O(1/\ln(1/\phi))$ smaller than the displacements caused by a single fibre. The rate of two-fibre interactions is $O(\ln(1/\phi))$ larger than the rate of single-fibre interactions. Thus, using (3), we find that the contributions of two-fibre correlations to $D^*$ are $O(1/\ln(1/\phi))$ smaller than the leading contribution.

We must now determine the concentration disturbance $\langle c' \rangle_1$ produced by a fibre. Taking the conditional average of (12) at steady state and subtracting (13) gives

$$\nabla \cdot [\langle \boldsymbol{u} \rangle \langle c' \rangle_1 + \langle \boldsymbol{u}' \rangle_1 \langle c \rangle + \langle \boldsymbol{u}' \rangle_1 \langle c' \rangle_1 + \langle \boldsymbol{u}'' c'' \rangle_1 - D \nabla \langle c' \rangle_1] = 0, \tag{18}$$

where $\boldsymbol{u}'' = \boldsymbol{u} - \langle \boldsymbol{u} \rangle_1$ and $c'' = c - \langle c \rangle_1$. The product $\langle \boldsymbol{u}' \rangle_1 \langle c' \rangle_1$ is $O(1/\ln(1/\phi))$ smaller than $\langle \boldsymbol{u} \rangle \langle c' \rangle_1$ and will be neglected. The order of magnitude of $\langle \boldsymbol{u}'' c'' \rangle_1$ may be estimated by making a self-consistent approximation in which this term is modelled in the same way as the term $\langle \boldsymbol{u}' c' \rangle_1$ that appears in the unconditionally averaged mass conservation equation, i.e.

$$\langle \boldsymbol{u}'' c'' \rangle_1 \approx -\boldsymbol{D}^* \cdot \nabla \langle c' \rangle_1, \tag{19}$$

where $\boldsymbol{D}^*$ is the hydrodynamic diffusivity tensor whose $yy$-component has been denoted by $D^*$. Using (19), and taking account of the facts that the mean concentration varies only in the $y$-direction and the mean velocity has a non-zero component only in the $x$-direction, equation (18) becomes

$$\langle u_x \rangle \frac{\partial \langle c' \rangle_1}{\partial x} - \nabla \cdot [(D\boldsymbol{I} + \boldsymbol{D}^*) \cdot \nabla \langle c' \rangle_1] = -\langle u'_y \rangle_1 \frac{\mathrm{d}\langle c \rangle}{\mathrm{d}y}. \tag{20}$$

The diffusion terms in (20) may be neglected if the diffusion results in a small change of the tracer's $y$-coordinate in the interaction time $\tau = \xi^2/(Uy)$. The displacement of the tracer due to hydrodynamic diffusion is $(D^*\tau)^{1/2} = O(y/\ln^{1/2}(1/\phi))$, where use has been made of (6) and (2) in obtaining the latter estimate. Thus, the hydrodynamic

diffusivity always leads to a displacement of the tracer during an interaction that is small compared with its separation from the wall. The molecular diffusivity may lead to a large relative displacement of the tracer at very small separations from the wall where $D \gg D^*$. However, we will only be interested in calculating $D^*$ in the region where it makes a significant contribution to the mean flux. Since the concentration gradient is nearly constant over the distances, $\Delta y = O(y/\ln(1/\phi))$, through which a tracer is transported during its interaction with a fibre, the mean concentration gradient in (20) may be approximated as a constant and integrating this equation gives

$$\langle c' \rangle_1 = \frac{-d\langle c \rangle / dy}{\langle u_x \rangle (y)} \int_{-\infty}^{x} dx' \langle u_y' \rangle_1 (x' - x_w, y, z - z_w). \tag{21}$$

Combining (21) with (17) gives

$$D^* = \int d\boldsymbol{e} \frac{\phi e_y}{\pi^2 a^2 \langle u_x \rangle (y)} \int dx_w \, dz_w \langle u_y' \rangle_1 (x - x_w, y, z - z_w) \int_{-\infty}^{x} dx' \langle u_y' \rangle_1 (x' - x_w, y, z - z_w). \tag{22}$$

Integrating (22) by parts with respect to $x_w$, we obtain

$$D^* = \int d\boldsymbol{e} \frac{\phi e_y}{2\pi^2 a^2 \langle u_x \rangle (y)} \int_{-\infty}^{\infty} dz_w \left( \int_{-\infty}^{\infty} dx_w \langle u_y' \rangle_1 (x - x_w, y, z - z_w) \right)^2. \tag{23}$$

It is convenient to express the diffusivity in terms of the Fourier transform of the velocity field with respect to the $x$- and $z$-coordinates. Using the product theorem, (23) may be written as

$$D^* = \int d\boldsymbol{e} \frac{\phi e_y}{2\pi^2 a^2 \langle u_x \rangle (y)} \int_{-\infty}^{\infty} dk_z \langle \hat{u}_y' \rangle_1 (k_x = 0, y, k_z) \langle u_y' \rangle_1 (k_x = 0, y, -k_z), \tag{24}$$

where $\hat{}$ denotes a Fourier transform with respect to $x$ and $z$ and $k_x$ and $k_z$ are the $x$- and $z$-components of the wavenumber. In writing (24), we have made use of the translational invariance in the $x$- and $z$-directions, i.e. $\langle u_y' \rangle_1$ is only a function of the position of the tracer relative to the point $\boldsymbol{r}_w$ of intersection of the fibre with the wall.

To complete the determination of the diffusivity, we must find the mean velocity as well as the conditional average velocity disturbance caused by a fibre. We assume that the Reynolds number $Re = \rho U \xi / \mu$ is very small, so that the fluid motion is governed by the Stokes equations. The ensemble average of the equations of motion can be approximated as Brinkman's equations

$$\mu \nabla^2 \langle \boldsymbol{u} \rangle - \nabla \langle p \rangle - (\mu / \xi^2) \langle \boldsymbol{u} \rangle = 0, \tag{25}$$

$$\nabla \cdot \langle \boldsymbol{u} \rangle = 0, \tag{26}$$

where the Brinkman screening length $\xi$ is given by (2). The term $(\mu/\xi^2)\langle \boldsymbol{u} \rangle$ arises due to the force per unit volume that the fibres exert on the fluid. In using (25) with (2), we have neglected the effect of interactions with the wall on the force per unit length exerted by a fibre. The dominant effect of the fibres on $\langle \boldsymbol{u} \rangle (y)$ comes from fibres with separations of $O(\xi)$ or larger even when $y \ll \xi$. (In fact, (25) and (26) could be approximated by the Stokes equations for $y \ll \xi$.) Thus, the neglect of wall reflections results in relative errors of $O(1/\ln(\xi/a))$. The force dipole and higher-order multipoles distributed along the fibre axis have also been neglected. The effect of these terms is small, $O(a^2/\xi^2)$ for a velocity field that is varying on a length scale $\xi$. These estimates indicate that wall reflections and higher-order multipoles can be neglected at

asymptotically small volume fractions for which $\xi/a \gg 1$. An assessment of the accuracy of Brinkman's equation near the boundaries between fininte-volume-fraction periodic fixed beds and pure fluid regions has been given by Larson & Higdon (1986, 1987) and Sangani & Behl (1989).

We consider a unidirectional average flow field in the $x$-direction driven by a constant pressure gradient $\nabla\langle p\rangle = -\mu U/\xi^2 \boldsymbol{e}_x$. The solution of (25) driven by this pressure field and satisfying a no-slip boundary condition at the solid surface $y = 0$ is

$$\langle u_x\rangle = U[1-\exp(-y/\xi)]. \tag{27}$$

The conditional average of the equations of motion with one fibre's position and orientation held fixed takes a form analogous to (25) and (26) with errors that are small at low volume fractions. In a dilute fixed bed, interparticle interactions are only important at $O(\xi)$ inter-fibre separations where the conditional average velocity is slowly varying and the effects of the surrounding fibres can be modelled in terms of a body force. If we denote the deviations of the pressure and velocity fields from the average by $p' = p-\langle p\rangle$ and $\boldsymbol{u}' = \boldsymbol{u}-\langle \boldsymbol{u}\rangle$, then we can write equations for the velocity and pressure disturbance caused by a fibre as

$$-\mu\nabla^2\langle \boldsymbol{u}'\rangle_1 + (\mu/\xi^2)\langle \boldsymbol{u}'\rangle_1 + \nabla\langle p'\rangle_1 = \int_0^\infty \mathrm{d}s\langle \boldsymbol{f}\rangle_1(\boldsymbol{r}_w+s\boldsymbol{e})\,\delta(\boldsymbol{r}-\boldsymbol{r}_w-s\boldsymbol{e}), \tag{28}$$

$$\nabla\cdot\langle \boldsymbol{u}'\rangle_1 = 0, \tag{29}$$

The force per unit length acting on the fibre, $\langle \boldsymbol{f}\rangle_1$, is, cf. Koch & Brady (1986) and Spielman & Goren (1968),

$$\langle \boldsymbol{f}\rangle_1 = \frac{-6\pi\mu a^2}{5\phi\xi^2}[\boldsymbol{I}-\tfrac{1}{2}\boldsymbol{ee}]\cdot\langle \boldsymbol{u}\rangle(s\boldsymbol{e}_y). \tag{30}$$

In writing (30), we have neglected the effect of reflections with the wall on the force per unit length, leading to $O(1/\ln(\xi/a))$ relative errors.

The velocity disturbance caused by a fibre in the presence of the plane solid boundary can be written as the sum of the velocity produced by a fibre in an unbounded fluid, $\boldsymbol{u}^u$, and a homogeneous solution $\boldsymbol{u}^h$ of Brinkman's equations chosen to satisfy the boundary conditions on the solid boundary, i.e.

$$\langle \boldsymbol{u}'\rangle_1 = \boldsymbol{u}^u + \boldsymbol{u}^h. \tag{31}$$

The unbounded velocity disturbance can be written in terms of an integral over the fibre length of the force per unit length acting on the fibre times the Green's function $\boldsymbol{J}$:

$$\boldsymbol{u}^u = \int_0^\infty \mathrm{d}s\,\langle \boldsymbol{f}\rangle_1(s\boldsymbol{e}_y)\cdot\boldsymbol{J}(\boldsymbol{r}|\boldsymbol{r}_w+s\boldsymbol{e}). \tag{32}$$

The fundamental solution of Brinkman's equation, $\boldsymbol{J}$, satisfies

$$-\mu\nabla^2\boldsymbol{J} + (\mu/\xi^2)\boldsymbol{J} + \nabla\boldsymbol{P} = \boldsymbol{I}\delta(\boldsymbol{r}-\boldsymbol{r}_w-s\boldsymbol{e}), \tag{33}$$

$$\nabla\cdot\boldsymbol{J} = 0, \tag{34}$$

where $\boldsymbol{J}\cdot\boldsymbol{f}$ and $\boldsymbol{P}\cdot\boldsymbol{f}$ are the velocity and pressure fields due to a point force $\boldsymbol{f}$ exerted on the fluid at $\boldsymbol{r}_w+s\boldsymbol{e}$. The solution for $\boldsymbol{J}$ can be obtained by taking the three-dimensional Fourier transform of (33) and (34) to give

$$\boldsymbol{J} = \int \mathrm{d}\boldsymbol{k}\,\frac{\boldsymbol{I}-\boldsymbol{kk}/k^2}{\mu[(2\pi k)^2+\xi^{-2}]}\exp[2\pi\mathrm{i}\boldsymbol{k}\cdot(\boldsymbol{r}-\boldsymbol{r}_w-s\boldsymbol{e})], \tag{35}$$

where $\boldsymbol{k} = (k_x, k_y, k_z)$ is the three-dimensional Fourier transform variable. To determine the diffusivity from (28), we require the two-dimensional Fourier transform of the $y$-component of the velocity disturbance evaluated at $k_x = 0$. Thus, we need to consider the two-dimensional Fourier transforms of $J_{xy}$, $J_{yy}$, and $J_{zy}$. It may be seen from (35) that $\hat{J}_{xy}(k_x = 0) = 0$. Performing the inverse Fourier transform of the other two components with respect to $k_y$ yields

$$\hat{J}_{yy}(k_x = 0) = \frac{\xi}{2\mu}\left(\frac{-\alpha^2}{\beta}\exp[-\beta|y - se_y|] + |\alpha|\exp[-|\alpha||y - se_y|]\right), \tag{36}$$

$$\hat{J}_{zy}(k_x = 0) = \frac{\mathrm{i}\alpha\,\mathrm{sgn}(y - se_y)}{2\mu}(\exp[-\beta|y - se_y|] - \exp[-|\alpha||y - se_y|]), \tag{37}$$

where $\alpha = 2\pi k_z \xi$, $\beta \equiv (\alpha^2 + 1)^{1/2}$, and $s$ and $y$ in these and all subsequent expressions in this section are non-dimensionalized by $\xi$.

Substituting (36), (37), (27) and (30) into the Fourier transform of (32) and integrating with respect to $s$ gives

$$\hat{u}_y^u = \frac{-3\pi a^2 U e_x}{5\phi\xi^2} B^u, \tag{38}$$

where

$$B^u = [b_1 + b_4\exp(-y)]\exp(-\mathrm{i}\alpha\eta y) + b_2\exp(-\beta y) + b_3\exp(-|\alpha|y), \tag{39}$$

$\eta = e_z/e_y$, and the coefficients $b_i$ are given by

$$b_1 = \frac{2}{\beta^2 + \alpha^2\eta^2}, \tag{40}$$

$$b_2 = \frac{\alpha^2(1+\eta^2) - \mathrm{i}\alpha\eta/\beta}{\beta^2 + \alpha^2\eta^2} + \frac{\alpha^2(1+\eta^2) - \alpha^2/\beta + \mathrm{i}\alpha\eta(1/\beta - 1)}{(\beta - 1)^2 + \alpha^2\eta^2}, \tag{41}$$

$$b_3 = -1 + \frac{\alpha^2(1+\eta^2) - |\alpha| + \mathrm{i}\alpha\eta}{(|\alpha| - 1)^2 + \alpha^2\eta^2}, \tag{42}$$

$$b_4 = \frac{\alpha^2(1+\eta^2) + \alpha^2/\beta + \mathrm{i}\alpha\eta(1 + 1/\beta)}{(\beta + 1)^2 + \alpha^2\eta^2} + \frac{\alpha^2(1+\eta^2) - \alpha^2/\beta - \mathrm{i}\alpha\eta(1/\beta - 1)}{(\beta - 1)^2 + \alpha^2\eta^2}$$
$$+ \frac{|\alpha| - \alpha^2(1+\eta^2) - \mathrm{i}\alpha\eta}{(|\alpha| - 1)^2 + \alpha^2\eta^2} - \frac{\alpha^2(1+\eta^2) + |\alpha| + \mathrm{i}\alpha\eta}{(|\alpha| + 1)^2 + \alpha^2\eta^2}. \tag{43}$$

To satisfy the no-slip conditions on the boundary to the fixed bed, we must add to $\boldsymbol{u}^u$ a solution of the homogeneous Brinkman equations, $\boldsymbol{u}^h$. The homogeneous pressure $p^h$ and velocity $\boldsymbol{u}^h$ satisfy equations equivalent to (25) and (26). Combining (25) and (26), it can be seen that $p^h$ satisfies Laplace's equation, which upon Fourier transforming with respect to $x$ and $z$ gives

$$\frac{\mathrm{d}^2\hat{p}^h}{\mathrm{d}y^2} - (2\pi K)^2\hat{p}^h = 0, \tag{44}$$

where $K \equiv (k_x^2 + k_z^2)^{1/2}$. The solution of (44) that decays at large separations from the wall is

$$\hat{p}^h = \frac{-3\lambda_1\mu a^2 U e_x}{10K\phi\xi^4}\exp(-2\pi K y). \tag{45}$$

The Fourier transform of the $y$-component of the momentum conservation equation is

$$-\mu\frac{\mathrm{d}^2u_y^h}{\mathrm{d}y^2}+\mu\beta^2u_y^h+\frac{\mathrm{d}p^h}{\mathrm{d}y}=0. \tag{46}$$

The solutions of (46) that decay at large $y$ are

$$\hat{u}_y^h(k_x=0)=\frac{-3\pi a^2Up_x}{5\phi\xi^2}B^h, \tag{47}$$

where

$$B^h=\lambda_1\exp(-|\alpha|y)+\lambda_2\exp(-\beta y). \tag{48}$$

The constants $\lambda_1$ and $\lambda_2$ may be evaluated by applying the no-slip boundary conditions:

$$\langle\hat{u}_y'\rangle_1=0 \quad \text{at} \quad y=0, \tag{49}$$

$$\frac{\mathrm{d}\langle\hat{u}_y'\rangle_1}{\mathrm{d}y}=0 \quad \text{at} \quad y=0. \tag{50}$$

The second condition, (50), can be derived from the conditions of zero tangential velocity, $\langle u_x'\rangle_1=\langle u_z'\rangle_1=0$ and the Fourier transform of the mass conservation equation. The constants are found to be

$$\lambda_1=(\beta q_2+q_1)/(|\alpha|-\beta), \tag{51}$$

$$\lambda_2=(|\alpha|q_2+q_1)/(\beta-|\alpha|), \tag{52}$$

where

$$q_2=b_1+b_2+b_3+b_4, \tag{53}$$

$$q_1=-\mathrm{i}\alpha\eta b_1-\beta b_2-|\alpha|b_3-(1+\mathrm{i}\alpha\eta)b_4. \tag{54}$$

Substituting (31), (38) and (47) into (24), defining a spherical coordinate system in which $e_y=\sin\theta\sin\Phi$, $e_x=\cos\theta$, and $e_z=\sin\theta\cos\Phi$, and integrating over $\theta$ gives the following expression for the hydrodynamic diffusivity:

$$D^*=\frac{9Ua^2}{800\xi\phi}J=\frac{4}{\pi^2}D_\infty^*J, \tag{55}$$

where

$$J\equiv\int_0^1\mathrm{d}\zeta\int_0^\infty\mathrm{d}\alpha\,B(\alpha)\,B(-\alpha), \tag{56}$$

$$B\equiv B^u+B^h, \quad \zeta=\cos\Phi, \quad \text{and} \quad \eta^2=\zeta^2/(1-\zeta^2).$$

The integrals in (56) were evaluated numerically to determine the hydrodynamic diffusivity. The diffusivity normalized by its value, $D_\infty^*$, at large separations from the wall is plotted as a function of the non-dimensional separation $y$ in figure 1. For $y\ll 1$, $D^*/D_\infty^*=0.29y^3$ in agreement with the scaling prediction (6) with $d_1'=0.29$ or $d_1=0.008\,05$; this asymptote is plotted as the dashed line in figure 1. Owing to the long-range nature of the velocity perturbations produced by long straight fibres (even in the presence of Brinkman screening), the effect of the wall on the diffusivity decays slowly and $D^*/D_\infty^*\approx 1-1.37/y$ for $y\gg 1$.

In order to determine the concentration decrease, $\langle c\rangle(y=H)-\langle c\rangle(y=0)$, between two walls of a fixed bed, we require an approximation, $D_2^*(y)$, for the hydrodynamic diffusivity that takes account of the influence of both walls. At large

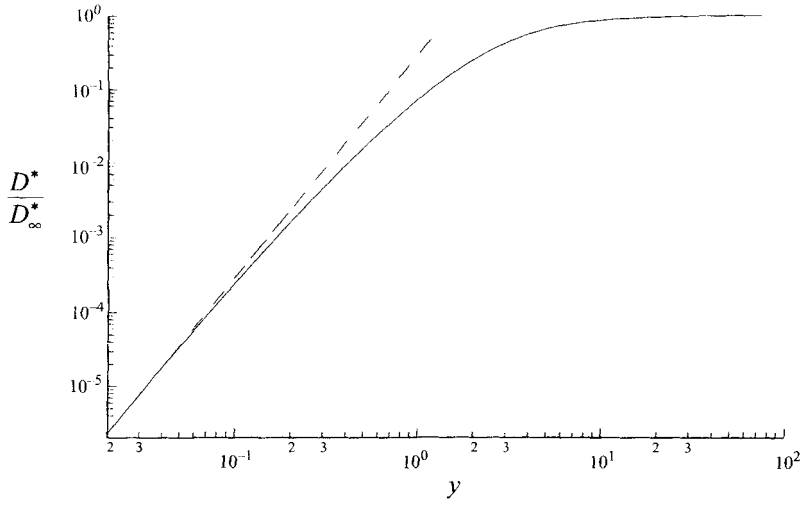


FIGURE 1. The ratio of the hydrodynamic diffusivity in an isotropic fixed-fibre bed, $D^*$, to its value at asymptotically large separations from the wall, $D^*_\infty$, is plotted as a function of the distance, $y$, from the wall non-dimensionalized with the screening length. The dashed line indicates the asymptotic behaviour $D^*/D^*_\infty = 0.29y^3$.

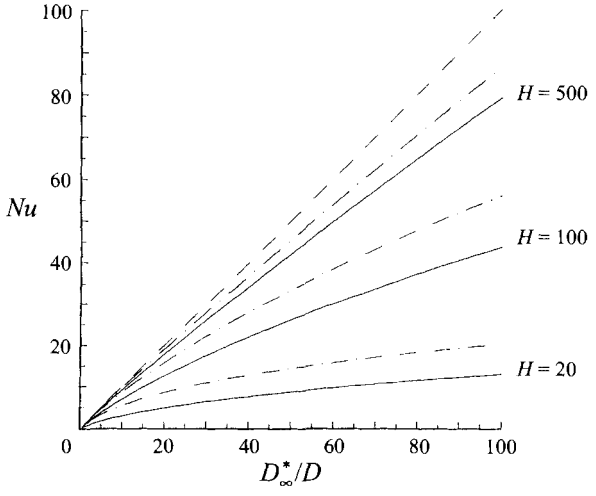


FIGURE 2. The Nusselt number, $Nu = hH/D$, for transport between two parallel walls bounding a fixed-fibre bed is plotted as a function of $D^*_\infty/D$. Results are shown for three values of the bed width non-dimensionalized by the screening length, $H = 20$, 100 and 500. The solid lines are the theoretical predictions (55). The dash-dot lines are the approximation (11), which only takes account of the boundary-layer and bulk resistances. The dashed line indicates the Nusselt number in the absence of boundary effects, i.e. $Nu = D^*_\infty/D$.

separations from both walls, one can superimpose the small decrease in diffusivity caused by each of the two walls. Close to either wall, the diffusivity is dominated by the nearby wall. Thus, a uniformly valid approximation may be obtained using $D^*_2 = D^*(y)\,D^*(H-y)/D^*_\infty$. Substituting $D^*_2$ for the hydrodynamic diffusivity in (17), integrating to obtain the concentration decrease, and using (9), we obtained the results plotted as solid lines in figure 2. For comparison, we also present as dash-dot lines the

approximation, (11), for the Nusselt number that takes into account only the boundary layer and bulk resistances to mass transport. The relative error incurred in using (11) decays like $\ln(H)/H$ as the width of the bed, $H$, approaches infinity. An $O(1/H)$ error arises from the neglect of the added resistance associated with the attenuation of the diffusivity at $O(1)$ separations from the wall, while the $O(\ln(H)/H)$ error arises from the slowly decaying $O(1/y)$ influence of the wall on the diffusivity for $y \gg 1$. The dashed line in figure 2 shows the Nusselt number, $Nu = D^*_\infty/D$, that would arise in the absence of wall effects. It may be seen that a very large bed is required to make wall effects negligible and the required bed size increases with increasing $D^*_\infty/D$ or, equivalently, increasing Péclet number.

## 3. Dispersion in a sheared suspension of neutrally buoyant spheres

Phenomena similar to those described above may also be expected to occur in free suspensions. As an example, we will consider heat or mass transfer across a sheared suspension of neutrally buoyant spheres. The shear is driven by two parallel solid walls separated by a distance $H$, which is large compared with the particle radius $a$. We are interested in the transport of heat or mass from one wall to the other at a statistically stationary state.

It is well known from the experimental measurements of Leighton & Acrivos (1987), the numerical simulations of Bossis & Brady (1988) and Brady & Phung (1992), and a theoretical calculation of Wang, Mauri & Acrivos (1995) that the effective self-diffusion coefficient for the motion of a marked non-Brownnian solid particle parallel to the gradient ($y$-) direction in a sheared suspension is proportional to $\gamma a^2$ as expected on the basis of dimensional analysis. Furthermore, the effective diffusivity is proportional to $\phi^2$ at small solid volume fractions $\phi$. Stokes flow reversibility together with the fore-aft symmetry of the flow situation imply that two-particle interactions cannot lead to a net displacement $\Delta y$ of the tracer particle. The symmetry is broken when the tracer particle encounters a pair of other particles and the frequency of such encounters is proportional to $\phi^2$.

The same considerations will apply to the scaling of the effective diffusivity of a fluid-phase tracer molecule whose diffusivity is very small so that $Pe_\gamma \gg 1$. Thus, the hydrodynamic diffusivity far from the walls is given by

$$D^* = D^*_\infty = d_2 \gamma a^2, \quad y \gg a, \quad H - y \gg a, \tag{57}$$

where $d_2$ is a dimensionless function of volume fraction and is proportional to $\phi^2$ in the dilute limit, $\phi \ll 1$. It should be noted, however, that $d_2$ will differ from the corresponding function, $d_s$, for hydrodynamic diffusion of solid particles because the solid particles are not passive tracers.

Now let us turn to the scaling of the hydrodynamic diffusivity of a fluid-phase tracer molecule near the solid boundary. We will estimate the diffusivity as the product of the interaction rate $R$ and the square of the tracer displacement, $\Delta y$, caused by each interaction, cf. (3). A tracer molecule's velocity is influenced by solid particles that are separated from it by a distance of $O(a)$. These particles are swept past its position in a time $\tau = O(\gamma^{-1})$. An interaction with a single solid particle will not produce a net displacement of the tracer molecule, so at least two particles must simultaneously interact with the tracer to contribute to the diffusivity. Thus, $R = O(\gamma\phi^2)$ in a dilute suspension and $R = O(\gamma)$ for $\phi \sim O(1)$. The no-slip boundary condition and the continuity equation require that the normal component, $u'_y$, of the velocity disturbance caused by the particles goes to zero quadratically as one approaches the wall, $y \to 0$.

Thus, $u_y' = O(\gamma y^2/a)$ and the net displacement is $\Delta y = O(u_y'\tau) = O(y^2/a)$. It may be noted that $\Delta y/y = O(y^2/a^2) \ll 1$, validating a local description of the hydrodynamic diffusion at small separations from the wall, $y \ll a$, even in a concentrated suspension. Substituting these scalings into (5), the hydrodynamic diffusivity near the wall of a sheared suspension is

$$D^* = d_3 \gamma y^4/a^2, \quad y \ll a, \tag{58}$$

where $d_3$ is a dimensionless function of $\phi$ that is proportional to $\phi^2$ at small volume fractions. The hydrodynamic diffusivity will be comparable with the molecular diffusivity in a boundary layer of thickness $\epsilon = aPe_\gamma^{-1/4}$ near the wall at high Péclet numbers.

Now, let us consider an average concentration field that is steady and only depends on the $y$-coordinate. The mean flux $Q$ resulting from the combined effects of hydrodynamic (58) and molecular diffusion is constant:

$$Q = D\left(d_3 \frac{y^4}{\epsilon^4} + 1\right)\frac{\mathrm{d}\langle c\rangle}{\mathrm{d}y}, \quad y \ll a. \tag{59}$$

Integrating (59) over $y$, we can obtain the concentration slip in the boundary layer:

$$\Delta c = \langle c\rangle(a \gg y \gg \epsilon) - \langle c\rangle(y = 0) = \frac{\pi Q \epsilon}{2^{3/2} d_3^{1/4} D} = \frac{\pi Q a}{2^{3/2}(d_3 Pe_\gamma)^{1/4}}. \tag{60}$$

The concentration gradient in the bulk of the suspension is $Q/D_\infty^* = Q/(d_2 \gamma a^2)$. Provided that $H/a \gg 1$ and $\epsilon \ll a$, the concentration difference across the gap may be approximated as

$$\langle c\rangle(y = H) - \langle c\rangle(y = 0) = 2\Delta c + QH/D_\infty^*. \tag{61}$$

Substituting (60) and (61) into (9) yields

$$\frac{1}{Nu} = \frac{1}{d_2 Pe_\gamma} + \frac{\pi a}{2^{1/2} H (d_3 Pe_\gamma)^{1/4}}. \tag{62}$$

From (62), it may be seen that the heat transfer coefficient is approximately equal to the bulk hydrodynamic diffusivity divided by the gap thickness when $H/a \gg Pe_\gamma^{3/4} \gg 1$ and is controlled by the boundary layer resistance when $Pe_\gamma^{3/4} \gg H/a \gg 1$.

Wang & Keller (1985) used an electrochemical technique to measure the diffusion of ions from one cylinder of a Couette device to the other. The gap of the Couette device was filled with a suspension of hardened human red blood cells, which behave approximately as hard spheres of radius 4.2 μm (see Zydney & Colton 1988). The gap of the Couette device was 460 μm, so that $H/a = 110$. The ions did not permeate the particles. It was found that shearing the suspension gave rise to an enhancement of the transport that could be considered to be almost purely hydrodynamic. However, the growth of the Nusselt number was slightly slower than linear with shear rate and this might indicate small effects of boundary layer resistance.

Sohn & Chen (1981) measured the heat transfer between the inner and outer cylinders of a Couette device containing a neutrally buoyant suspension of polyethylene spheres in a mixture of silicone oil and kerosene. The ratio of the gap thickness to the particle radius was only 18 in this study and the augmentation of the heat transfer caused by the shear and was significantly less than the augmentation of the mass transfer in Wang & Keller's experiment. Sohn & Chen also observed that the augmentation of the heat transfer due to shear was much larger with a suspension of smaller polystyrene spheres for which $H/a = 180$ than for the large polyethylene

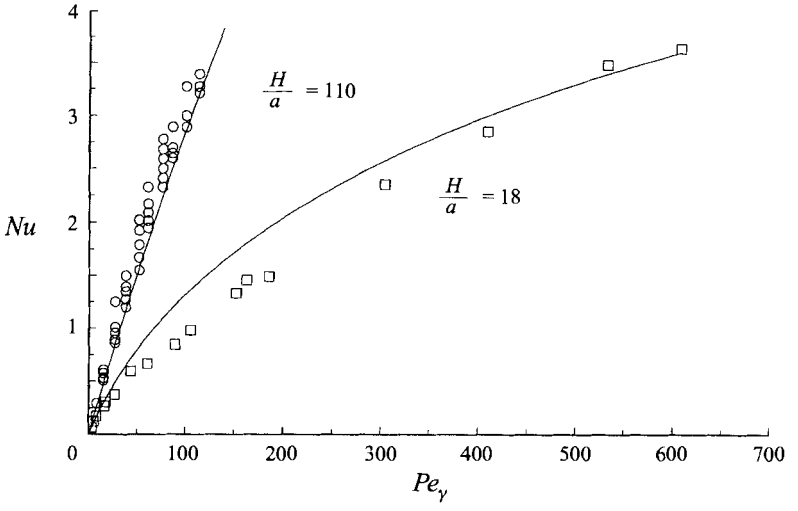


FIGURE 3. The Nusselt number in a moderately dilute sheared suspension. The solid lines indicate the theoretical prediction (62). The squares are the experimental data of Sohn & Chen (1981) for $\phi = 0.15$ and $H/a = 18$ and the circles are the experiments of Wang & Keller (1985) for $\phi = 0.18$ and $H/a = 110$.

spheres. However, the data for the small spheres was limited to $Pe_\gamma < 10$. The lower heat transfer coefficient observed in Sohn & Chen's experiments with polyethylene spheres may be attributed to the increased importance of the boundary layer resistance for a smaller value of $H/a$.

Before turning to a comparison of the theory with the experimental results, we should note three complicating factors that limit the quantitative significance of this comparison. First, our theory for simple shear flow only considers the bulk and boundary layer resistances to transport. It does not include effects of the hydrodynamic diffusion at $O(a)$ distances from the wall, which is likely to have an effect on $Nu$ at finite $Pe_\gamma$ and $H/a$. Some indication of the likely size of this effect may be obtained by observing the accuracy of the comparable approximation in the fixed bed problem, cf. figure 2. Second, we have only developed a scaling analysis for the hydrodynamic diffusion and boundary layer resistance and have not determined the values of $d_2(\phi)$ and $d_3(\phi)$. Thus, these coefficients must be treated as fitting parameters in the comparison with the experimental data. A more definitive test of the theory would be possible if numerical simulations were used to obtain one or both of these coefficients. Finally, the heat and mass transfer experiments differ in that heat can be carried by the particle phase whereas the ions cannot. (The heat capacity of the particles in Sohn & Chen's experiment is about 1.5 times that of the fluid.) Since the volume fraction of solids goes to zero in the boundary layer, this will not affect $d_3$ but it will lead to a difference between the values of $d_2$ in the heat and mass transfer experiments at the same value of $\phi$. In a dilute suspension, the transport of heat carried inside particles scales like $\phi^3$ and is small compared with the $O(\phi^2)$ transport of heat in the fluid phase. In practice, we will neglect the effect of the heat transport in the particle phase on $d_2$ even at $\phi = 0.15$ and $\phi = 0.3$. By so doing, we can determine whether the same values of $d_2$ and $d_3$ are able to explain the quite different qualitative trends observed in the heat and mass transfer experiments.

The Nusselt number representing the enhancement of transport due to shearing motion is plotted as a function of $Pe_\gamma$ in figures 3 and 4 for relatively dilute suspensions

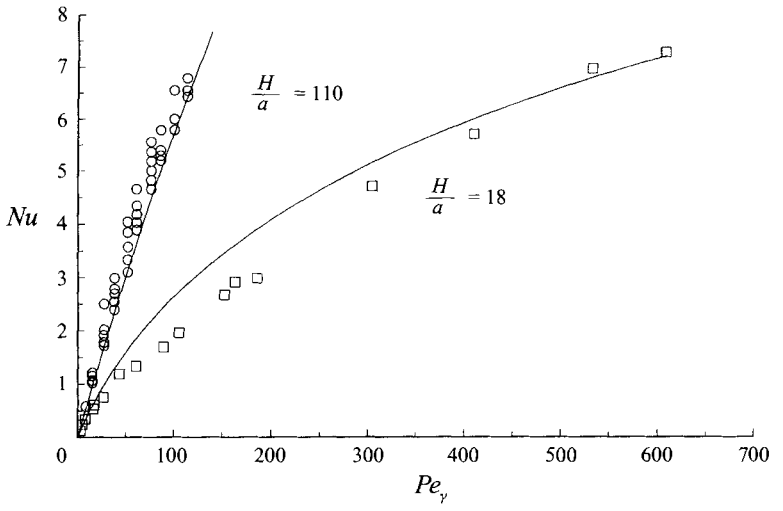


FIGURE 4. The Nusselt number in a concentrated sheared suspension. The solid lines indicate the theoretical prediction (62). The squares are the experimental data of Sohn & Chen (1981) for $\phi = 0.30$ and $H/a = 18$ and the circles are the experiments of Wang & Keller (1985) for $\phi = 0.31$ and $H/a = 110$.

$\phi = 0.15$–$0.18$ and moderately concentrated suspensions $\phi = 0.3$–$0.31$, respectively. In each figure, the circles represent the experimental data for mass transfer with $H/a = 110$ obtained by Wang & Keller (1985) and the squares the heat transfer experiments of Sohn & Chen (1981) with $H/a = 18$. The solid lines in the figures are the results of the scaling analysis (62) with the constants chosen to give a good fit to the data.

In the theoretical analysis, we neglected the transport through the bulk of the suspension caused by molecular diffusion compared with the hydrodynamic diffusion as the effect of molecular diffusion is small for $Pe_\gamma \gg 1$. However, since the experiments were performed at moderate values of $Pe_\gamma$, we have interpreted $h$ as the difference between the mass transfer coefficient in the sheared suspension and that in a stagnant suspension. The effective diffusivity of the stagnant suspension was obtained using the empirical correlation developed by Meredith & Tobias (1961), which has been shown to compare favourably with experiments and numerical simulations (see Bonnecaze & Brady 1991) for volume fractions and conductivity ratios comparable with those used in the experiments.

The mass transfer experiments in figure 3 were conducted at a volume fraction of $\phi = 0.18$, whereas $\phi = 0.15$ for the heat transfer experiments. Since $d_2$ and $d_3$ are predicted to be proportional to $\phi^2$ in the dilute limit, the coefficients used to model the heat transfer experiments were chosen to be a factor of 1.44 smaller than those used to model the mass transfer experiments. The coefficients for the bulk and boundary layer diffusivity were $d_2 = 0.033$ and $d_3 = 0.0003$ at $\phi = 0.18$. The mass and heat transfer experiments presented in figure 4 were conducted for $\phi = 0.31$ and 0.30, respectively, and the coefficients $d_2 = 0.055$ and $d_3 = 0.003$ were used to model this data.

It can be seen from the figures that the scaling result, (62), is able to explain the nearly linear growth of the mass transfer rate with Péclet number as well as the much slower growth of the heat transfer rate. The smaller ratio of gap thickness to particle radius and the larger Péclet numbers in the heat transfer experiments lead to a relatively large contribution of the boundary layer to the overall resistance to transport

across the gap. While the quantitative significance of the comparison is limited by the factors mentioned above, it is clear that the experiments support the theoretical prediction for the qualitative nature of the boundary layer resistance.

The values of the bulk hydrodynamic diffusivity of a fluid-phase tracer obtained from our analysis of the experiments of Wang & Keller (1985) and Sohn & Chen (1981) are comparable with the values of the self-diffusivity of solid spheres measured by Leighton & Acrivos (1987). At $\phi = 0.18$, we obtained for the fluid-phase diffusivity $d_2 = D^*_\infty/(\gamma a^2) = 0.033$, while Leighton & Acrivos measured $d_s = 0.021$. At the higher volume fraction, $\phi = 0.31$, the fluid-phase diffusion coefficient is $d_2 = 0.055$, while the solid-particle coefficient is $d_s = 0.086$ (Leighton & Acrivos 1987). From this comparison, it appears that the fluid-phase diffusivity grows more slowly with solid concentration than does the solid-particle diffusivity. However, a more definitive determination of the relative size of the particle and fluid diffusivities could be made if both were measured in the same physical system or in the same numerical simulation.

## 4. Conclusion

In this paper, we have seen that the standard picture of purely hydrodynamic diffusion in fixed beds and suspensions at high Péclet numbers must be modified when we deal with heat or mass transfer from solid surfaces into the suspension or fixed bed. Whereas the random flow field is sufficient to account for the transport in the bulk of the suspension, molecular diffusion must play a role in transporting heat or mass through the nearly stagnant fluid adjacent to the wall. This principle has been illustrated with two specific examples.

The first case of dispersion into a dilute isotropic fixed fibrous medium has the advantage that it is amenable to analytical treatment. Using the method of averaged equations, we have derived the transverse hydrodynamic diffusivity as a function of the distance away from a solid boundary to the fibrous medium (figure 1). This result was then used to determine the net resistance to mass transfer across the bed over a range of Péclet numbers and fixed-bed sizes (figure 2). The mass transfer coefficient is nearly equal to $D^*_\infty/H$ for sufficiently large beds at intermediate Péclet numbers, $H/a \gg (Pe_a/\phi)^{2/3} \gg 1$. At very large Péclet numbers, $(Pe_a/\phi)^{2/3} \gg H/a$, the mass transfer resistance is controlled by a boundary layer near the solid surface and $h = 3^{3/2}(D^*_\infty D^2)^{1/3}/(4\pi\xi)$.

The second case considered is that of heat and mass transport in the direction of the gradient of the mean velocity in a sheared suspension of neutrally buoyant spheres. This case is interesting because of the experimental data available over a range of gap thicknesses $H/a$ and Péclet numbers. The mass transfer in a dilute sheared suspension results from an interaction of a pair of particles near a solid boundary with the fluid-phase tracer. Owing to the complexity of this problem, only scaling results were obtained for the diffusivity in a sheared suspension and the coefficients $d_2$ and $d_3$ were determined from the experimental data. The scaling analysis is able to explain the qualitative trends observed in the experiments. In particular, the Nusselt number is observed to grow nearly linearly with $Pe_\gamma$ for moderate values of $Pe_\gamma$ and large $H/a = 110$. However, the growth of $Nu$ is much slower for the smaller value of $H/a = 18$, especially at the largest values of $Pe_\gamma$. These trends are explained by the theory in terms of an increasing importance of the boundary layer resistance with increasing $Pe_\gamma$ and decreasing $H/a$.

A more quantitative test of the theory for transport into sheared suspension could be obtained by using numerical simulations to predict the hydrodynamic fluid-phase

diffusivity. In addition, it would be desirable to have a single experimental investigation that covers a wide range of $H/a$ without altering the physical properties of the particles and the method of measurement.

Financial support from NSF grant CTS-9526149 is gratefully acknowledged.

## REFERENCES

BONNECAZE, R. T. & BRADY, J. F. 1991 The effective conductivity of random suspensions of spherical particles. *Proc. R. Soc. Lond.* A **432**, 445.

BOSSIS, G. & BRADY, J. F. 1987 Self-diffusion of Brownian particles in concentrated suspensions under shear. *J. Chem. Phys.* **87**, 5437.

BRADY, J. F. & PHUNG, T. 1992 Microstructure fluids: Structure, diffusion and rheology of colloidal dispersions. In *Proc 1st Tohwa Symposium: Slow Dynamics in Condensed Matter* (ed. K. Kawasaki, M. Tokuyama & T. Kawakatsu). *AIP Conf. Proc.* Vol. 256, p. 391.

CHENG, P. & ZHU, H. 1987 Effects of radial thermal dispersion on fully-developed forced convection in cylindrical packed tubes. *Intl J. Heat Mass Transfer* **30**, 2373.

ECKERT, E. R. G. & DRAKE, R. M. 1972 *Analysis of Heat and Mass Transfer*. McGraw-Hill.

FRIED, J. J. & COMBARNOUS, M. A. 1971 Dispersion in porous media. *Adv. Hydrosci.* **7**, 169.

HOWELLS, I. D. 1974 Drag due to the motion of a Newtonian fluid through a sparse random array of small fixed rigid objects. *J. Fluid Mech.* **64**, 449.

KOCH, D. L. & BRADY, J. F. 1985 Dispersion in fixed beds. *J. Fluid Mech.* **154**, 399.

KOCH, D. L. & BRADY, J. F. 1986 The effective diffusivity of fibrous media. *AIChE J.* **32**, 575.

KOCH, D. L. & BRADY, J. F. 1987 A non-local description of advection-diffusion with application to dispersion in porous media. *J. Fluid Mech.* **180**, 387.

LARSON, R. E. & HIGDON, J. J. L. 1986 Microscopic flow near the surface of two-dimensional porous media. Part 1. Axial flow. *J. Fluid Mech.* **166**, 449.

LARSON, R. E. & HIGDON, J. J. L. 1987 Microscopic flow near the surface of two-dimensional porous media. Part 2. Transverse flow. *J. Fluid Mech.* **178**, 119.

LEIGHTON, D. & ACRIVOS, A. 1987 Measurement of self-diffusion in concentrated suspensions. *J. Fluid Mech.* **177**, 109.

MEREDITH, R. E. & TOBIAS, C. W. 1961 Conductivities in emulsions, *J. Electrochem. Soc.* **108**, 286.

SANGANI, A. S. & BEHL, S. 1989 The planar singular solutions of Stokes and Laplace equations and their application to transport processes near porous surfaces. *Phys. Fluids* A **1**, 21.

SHAQFEH, E. S. G. 1988 A nonlocal theory for the heat transport in composites containing highly conducting fibrous inclusion. *Phys. Fluids* **31**, 2405.

SOHN, C. W. & CHEN, M. M. 1981 Microconvective thermal conductivity in disperse two-phase mixtures as observed in a low velocity Couette flow experiment. *J. Heat Transfer* **103**, 47.

SPIELMAN, L. & GOREN, S. L. 1968 Model for predicting pressure drop and filtration efficiency in fibrous media. *Envir. Sci. Tech.* **2**, 279.

WANG, N.-H. L. & KELLER, K. H. 1985 Augmented transport of extracellular solutes in concentrated erythrocyte suspensions in Couette flow. *J. Colloid Interface Sci.* **103**, 210.

WANG, Y., MAURI, R. & ACRIVOS, A. 1995 Transverse shear-induced diffusion of spheres in a dilute suspension. *J. Fluid Mech.* (submitted).

ZYDNEY, A. L. & COLTON, C. K. 1988 Augmented solute transport in the shear flow of a concentrated suspension. *Physico-Chem. Hydrodyn.* **16**, 77.